PARP1: A Potential Molecular Marker to Identify Cancer During Colposcopy Procedures

Paula Demétrio de Souza França[1,2], Navjot Guru[1], Abigail R. Kostolansky[1,3], Audrey Mauguen[4], Giacomo Pirovano[1], Susanne Kossatz[1,5], Sheryl Roberts[1], Marcio Abrahão[2], Snehal G. Patel[6], Kay J. Park[7], Thomas Reiner*[1,8,9], and Elizabeth Jewell*[6]

[1]Department of Radiology, Memorial Sloan Kettering Cancer Center, New York, New York; [2]Department of Otorhinolaryngology and Head and Neck Surgery, Federal University of São Paulo, São Paulo, Brazil; [3]Department of Chemistry, Princeton University, Princeton, New Jersey; [4]Department of Epidemiology and Biostatistics, Memorial Sloan Kettering Cancer Center, New York, New York; [5]Department of Nuclear Medicine, University Hospital Klinikum Rechts der Isar and TranslaTUM, Technical University Munich, Munich, Germany; [6]Department of Surgery, Memorial Sloan Kettering Cancer Center, New York, New York; [7]Department of Pathology, Memorial Sloan Kettering Cancer Center, New York, New York; [8]Department of Radiology, Weill Cornell Medical College, New York, New York; and [9]Chemical Biology Program, Memorial Sloan Kettering Cancer Center, New York, New York

Despite efforts in prevention, cervical cancer still presents with a high worldwide incidence and remains a great problem in public health, especially in low-income countries. Screening programs, such as colposcopy with Papanicolaou testing, have greatly improved mortality rates. However, the agents currently used to delineate those lesions (topical application of acetic acid or Lugol iodine) lack specificity and sometimes can lead to unnecessary biopsies or even cervical excisions. A tool to enable in vivo histology to quickly and quantitatively distinguish between tumor, dysplastic tissue, and healthy tissue would be of great clinical interest. **Methods:** Here, we describe the use of PARPi-FL, a fluorescent inhibitor of poly[adenosine diphosphate-ribose]polymerase 1 (PARP1), which is a nuclear enzyme that is overexpressed in cancer when compared with the normal surrounding tissues. We exploit its use as an optical imaging agent to specifically target PARP1 expression, which was demonstrated to be higher in cervical cancer than the normal surrounding tissue. **Results:** After topical application of PARPi-FL on freshly excised cone biopsy samples, the nuclei of tumor cells emitted a specific fluorescent signal that could be visualized using a handheld fluorescence confocal microscope. **Conclusion:** This approach has the potential to improve in vivo identification of tumor cells during colposcopy examination, allowing a rapid, noninvasive, and accurate histopathologic assessment.

Key Words: PARPi-FL; cervical cancer; fluorescence-guided surgery; PARP1

J Nucl Med 2021; 62:941–948
DOI: 10.2967/jnumed.120.253575

Globally, cervical cancer is still a widespread disease and ranks as the second most frequent type of cancer among young women (between 20 and 45 y old) in low-income and lower-middle-income countries (*1*,*2*), where access to health-care providers and human papillomavirus (HPV) vaccination is scarce (*2*,*3*). Several technologies to improve prevention, screening, and detection of cervical cancer have recently been described in the literature, including new imaging tools (*4*–*7*) and molecular tests for HPV detection (*8*,*9*); however, they have yet to be approved for standard clinical practice. Visual inspection of the cervix after application of acetic acid or Lugol iodine is still widely used as the standard screening method, especially in resource-limited places (*4*). Although broadly used, this technique presents variable sensitivity and specificity for detecting precancerous lesions, mostly due to observer bias (*10*). More consistent results using acetic acid or Lugol iodine to guide biopsies are achieved with adequate provider training and continuous retraining (*11*). In addition, staining with acetic acid or Lugol iodine does not enable an in vivo cellular visualization of the cervix and is used mainly to guide biopsies. The final result depends on the histopathologic analysis of the tissue, usually available only days after the procedure.

A tool to enable quick and accurate distinction between malignant, in situ cervical intraepithelial neoplasia (CIN) carcinomas and healthy tissue in vivo, without the need for invasive biopsy, would be of great clinical interest. To address a possible solution, we turned to the topical application of PARPi-FL, a fluorescent poly[adenosine diphosphate-ribose]polymerase 1 (PARP1) inhibitor, along with use of a handheld confocal microscope, to enable immediate identification of invasive and in situ carcinoma at a cellular level. PARPi-FL is derived from the scaffold of olaparib, a PARP1 inhibitor that is currently being used mostly for the treatment of breast and ovarian cancer (*12*,*13*). PARPi-FL penetrates the nuclei of cells and emits a fluorescent signal that allows it to serve as a surrogate for PARP1 expression (*14*).

A previous report on oral squamous cell carcinoma demonstrated that PARP1 expression gradually increases as the tissue accumulates molecular alterations (*15*). In addition, reports indicate that PARP1 overexpression in cancer cells is so remarkable that it enables tumor delineation in several malignancies (*14*–*17*). Importantly, studies have shown that PARPi-FL can safely be administered as a topical solution (*15*,*18*) and has high tissue permeability (4.6 μm/s), accumulating within minutes in the nuclei of cancer cells (*19*), where it is retained for several hours, allowing its use as a tumor stain. PARPi-FL use as an imaging tracer is well established and has been reported both preclinically (*18*–*21*) and clinically (*15*) for several other tumor types. In this study, we examined PARP expression in cervical adenocarcinoma compared

Received Jul. 13, 2020; revision accepted Oct. 16, 2020.
For correspondence or reprints, contact: Elizabeth Jewell (jewelle@mskcc.org)
*Contributed equally to this work.
Published online Nov. 13, 2020.

with the normal surrounding tissue. In addition, we performed experiments on both a swine animal model and on patients' ex vivo cone biopsy samples to investigate the feasibility of in vivo detection of cervical cancer during colposcopy procedures.

MATERIALS AND METHODS

Chemicals

Commercially available compounds were used without further purification unless otherwise stated. Bio Ultra polyethylene glycol (PEG) 300, triethylamine, and trifluoroacetic acid were purchased from Sigma-Aldrich. A high-performance liquid chromatography (HPLC) and liquid chromatography–mass spectrometry grade of acetonitrile was obtained from Fischer Scientific. Water (18.2 MΩ cm^{-1} at 25° C) was obtained from an Alpha-Q Ultrapure water system from Millipore. PARP-NH precursor (4-(4-fluoro-3-(piperazine-1-carbonyl)benzyl)phthalazin-1(2H)-one) was purchased from AA Blocks and purified by HPLC before use and further synthesis. Bodipy-FL succinimidyl-ester was purchased from Invitrogen and used without further purification. PARPi-FL was kept as a 1.5 mM stock solution in 100% BioUltra PEG 300 and diluted to the final working concentration for the respective experiments. All reactions were magnetically stirred. HPLC purification and analysis was performed on a Shimadzu ultrafast liquid chromatography HPLC system equipped with a DGU-20A degasser, an SPD-M20A ultraviolet detector, an LC-20AB pump system, and a CBM-20A communication bus module.

PARPi-FL Synthesis

PARPi-FL was synthesized according to our previously described procedure (*22*). Briefly, Bodipy-FL succinimidyl-ester (1.0 equivalent) was conjugated to 4-(4-fluoro-3-(piperazine-1-carbonyl)benzyl) phthalazin-1(2H)-one (1.0 equivalent) in the presence of Et_3N (5.0 equivalents) in acetonitrile for 4 h at room temperature (20° C–25° C). It was purified by preparative HPLC (Atlantis T3 5-μm column, 4.6 × 250 mm, 1 mL/min, 5%–95% acetonitrile [0.1% trifluoroacetic acid] in 15 min) to afford PARPi-FL in 70%–79% yield as a red solid. Analytic HPLC analysis (Waters Atlantis T3 C18 column, 5 μm, 4.6 × 250 mm) showed the imaging agent to have high purity (>99%; retention time, 13.9 min). The identity of PARPi-FL was confirmed using electrospray ionization mass spectrometry (MS(+) m/z = 663.63 $[M + Na]^+$).

Animal Work

To demonstrate PARP1 expression in the basal cells of normal cervixes and to show that tissues would have PARPi-FL uptake, we developed an animal model using swine cervixes. Three Yorkshire female swine were purchased from Archer. A cold-knife cone biopsy was performed after euthanasia. The specimens were stained with PARPi-FL (tissue was submerged in a 100 nM solution: 1 μg of PARPi-FL in 15 mL of 30% PEG 300 in phosphate-buffered saline for 5 min) and then imaged using a handheld confocal microscope. After imaging, the specimens were routinely processed (formalin-fixed, paraffin-embedded) for hematoxylin and eosin (H&E) staining and PARP1 immunohistochemistry. All animal experiments were performed in accordance with protocols approved by the Institutional Animal Care and Use Committee of Memorial Sloan Kettering and followed the National Institutes of Health guidelines for animal welfare.

Handheld Confocal Fiberoptic Imaging

Images were acquired as previously described. Briefly, the FIVE2 (Optiscan) handheld confocal microscope acquires images by using a single channel for illumination and detection of PARPi-FL (488-nm excitation) and a lens numeric aperture of 0.3 (similar to a ×10 objective) with a field of view of 475 × 475 μm. The probe was in direct contact with the tissue to acquire images. Different depths were assessed (z-axis, 0–400 μm). For all experiments, we used a band-pass filter of 515–575 nm, 94%–100% laser power, and a scanning speed of 1 frame per second. The depth in which the image was acquired is specified in each figure.

Patient Population

Seven banked cases of cervical adenocarcinoma (no tissue with CIN was included in this analysis) were acquired from the Memorial Sloan Kettering tissue bank. In the operating room, freshly resected cone excisions (n = 3) or a clitoral biopsy (n = 1) was acquired. In all cases, the research was performed under Institutional Review Board approval and in accordance with the guidelines of the Declaration of Helsinki. Written informed consent had been obtained from all participants.

H&E Staining to Delineate Cervical Cancer Lesions

To delineate tumor versus normal tissue and further correlate the findings with immunohistochemistry, the slides were stained with H&E according to our previously described technique. Briefly, paraffin-embedded sections (5 μm each) were obtained from the tissue bank at Memorial Sloan Kettering and stained with H&E by the Memorial Sloan Kettering Molecular Cytology Core facility. The slides were further scanned (Mirax; 3DHISTECH) to allow for digital histologic analysis. All cases were reviewed by an experienced gynecologic pathologist, who delineated viable tumor and normal tissue.

PARP1 Immunohistochemistry

PARP1 immunohistochemistry was performed on a consecutive slide according to our previously described procedure (*18*), using an automated Discovery XT processor (Ventana Medical Systems). The anti-PARP1 rabbit monoclonal antibody (46D11; Cell Signaling Technology) specifically binds both human and mouse PARP1 (0.4 μg/mL). Briefly, anti-PARP1 antibody was incubated for 5 h, followed by 1 h of incubation with biotinylated goat antirabbit IgG (PK6106; Vector Labs) at 1:200 dilution. For immunohistochemistry detection, a 3,3′-diaminobenzidine detection kit (Ventana Medical Systems) was used according to the manufacturer's instructions; sections were counterstained with hematoxylin and cover-slipped with Permount (Fisher Scientific). Incubating with a rabbit IgG instead of the primary antibody controlled for nonspecific binding of the secondary antibody. H&E-stained slides were used to delineate tumor and normal tissue. Those same areas were used for PARP1 quantification using the consecutive slide. PARP1 quantification was performed on digitalized slides according to our previously described procedure (*15*). Briefly, the threshold for signal intensity in the 3,3′-diaminobenzidine (brown) and hematoxylin (blue, representing all tissue area) channels was determined using an automated script within Fiji (ImageJ) analysis software for all samples used in the quantitative analyses. Color deconvolution was used to separate blue and brown signals, and the thresholds were kept constant: 0–114 for 3,3′-diaminobenzidine and 0–235 for hematoxylin. The relative PARP1-positive area was calculated by dividing the brown (3,3′-diaminobenzidine) area by the blue (total tissue area).

PARPi-FL Staining Procedure for Ex Vivo Fresh Cervical Tissue

Staining was performed on the whole, freshly excised cone-biopsy specimen by submerging the tissue in a solution containing 1,000 nM PARPi-FL in 15 mL of 30% PEG 300 in phosphate-buffered saline for 5 min (rapid staining protocol). The specimen was further washed in phosphate-buffered saline for 1 min before imaging. After imaging, the specimens were processed according to the standard of care. A gynecologic pathologist confirmed the histologic results and provided an H&E slide and a slide for PARP1 immunohistochemistry. The personnel who performed PARP staining and analyses did not know the sample type or the pathologist's final report at the time of tissue analysis.

Quantification of PARPi-FL Signal Intensity

PARPi-FL signal intensity was quantified on a tumor and normal areas using Fiji software. The same window leveling was used for tumor and normal tissue for each patient. Fifteen ROIs in the tumor and 15 ROIs in the normal tissue were drawn. The intensity was calculated by averaging the values. Tumor-to-background ratio was calculated by dividing the average signal derived from tumor by the average signal derived from normal tissue.

Statistical Analysis

Statistical analysis of PARP1 expression was performed using R, version 3.6.0 (R Core Team), and Prism, version 8 (GraphPad Software). To compare PARP1 expression (ratio of PARP1 expression to total tissue area) between tumor, epithelium, and deep tissue, we used a linear regression with random intercept in order to account for the correlation between measurements from the same patient. The linear regression was done on the logarithm transformation of the ratio (to ensure no negative prediction). Results with a P value of 0.05 or less were considered statistically significant. Statistical analysis of PARPi-FL confocal fluorescence was performed using the Mann–Whitney test. Data points represent mean values, and error bars represent SDs.

RESULTS

PARPi-FL Imaging of Swine Cervical Tissue with a Handheld Confocal Microscope

To analyze the value of handheld confocal microscopy in cervical tissue, we evaluated 3 cervical cone biopsies from healthy swine (Fig. 1A), taking advantage of the physiologic PARP1 expression in the healthy basal layer of the cervical squamous mucosa (Fig. 1B). After staining, we observed a relatively weak but detectable PARPi-FL signal in the nuclei of the basal layer cells using the handheld confocal microscope (Fig. 1C). Confocal imaging showed a highly organized tissue layer, with a homogeneous nuclear population of the same size and shape. The corresponding histologic slides (H&E and PARP1 immunohistochemistry) confirmed that the nuclei of the basal layer of the cervical mucosa showed PARP1 expression, which was weaker than that in tumor tissue (Fig. 1B).

PARP1 Overexpression in Cervical Cancer When Compared with Normal Tissue in Slides from Banked Tissue

Slides were cut from banked paraffin-embedded tissue of cervical adenocarcinoma and were reviewed by a gynecologic pathologist to identify tumor and normal tissue using H&E as the gold standard. Immunohistochemistry was used for quantification of PARP1 levels within tumor and normal tissue. The data on PARP1 expression come from 7 patients with cervical adenocarcinoma, each having between 11 and 39 measurements (median, 33). No premalignant lesions were analyzed in this cohort. We found that PARP1 was overexpressed in cancer and that its expression was significantly higher than in the normal adjacent squamous mucosa (Fig. 2A). Mean PARP1 expression was also shown to be lower in healthy deep cervical stroma than in the normal squamous epithelium. This finding was expected because of physiologic proliferation of the cervical epithelium. Importantly, the expression was significantly lower in the epithelium than in tumor areas, allowing a clear differentiation between them (Fig. 2B; Supplemental Table 1 [supplemental materials are available at http://jnm.snmjournals.org]). When accounting for the repeated measurements per patient, using 1 as a reference coefficient value on the statistic model, the ratio of the PARP1-positive area to the total tissue area averaged 95% lower in benign squamous epithelium than in tumor and 99% lower in normal stroma than in tumor ($P < 0.001$; Supplemental Table 2). The ratio of the PARP1-positive area to the total tissue area averaged 77% lower in normal stroma than in benign squamous epithelium (95%CI, 0.18–0.30; $P < 0.001$). Figure 2C demonstrates the ratio distribution in tumor, squamous epithelium, and stroma.

Ex Vivo PARPi-FL Tumor Detection in Human Cervical Excisions and Clitoral Biopsy Samples

After confirming the feasibility of the technique in a preclinical large-animal model, we tested handheld confocal microscopy using PARPi-FL in human cone biopsies inside the operating room. Three patients who were scheduled to undergo cone biopsy because of suspected adenocarcinoma lesions had their surgical specimens stained and imaged before pathology assessment. Figure 3 shows the study workflow. Patient 1 (Fig. 4A) harbored an adenocarcinoma at the transformation zone, extending to the ectocervix (Fig. 4A). Confocal imaging of the tumor area presented a disorganized pattern of cell nuclei with different sizes and shapes, yielding a fluorescent signal of 83.57 ± 11.85 arbitrary units (a.u.). On the other hand, when imaging the normal mucosa, we

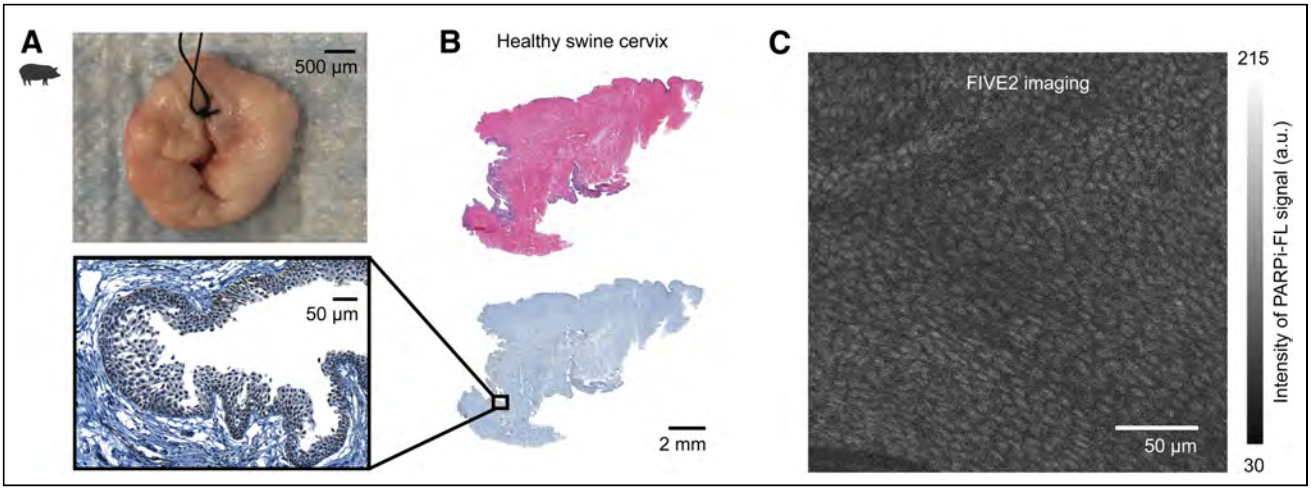

FIGURE 1. PARPi-FL imaging of healthy swine cervix. Physiologic PARP1 expression in cervical squamous basal layer allowed confocal imaging of healthy tissue in swine. (A) Cone biopsy obtained from 3 swine and stained with PARPi-FL. (B) H&E with corresponding immunohistochemistry demonstrating presence of PARP1. (C) Handheld confocal microscopy image showing cells arranged in layers with nuclei of same size and shape. Tissue depth is 10 µm.

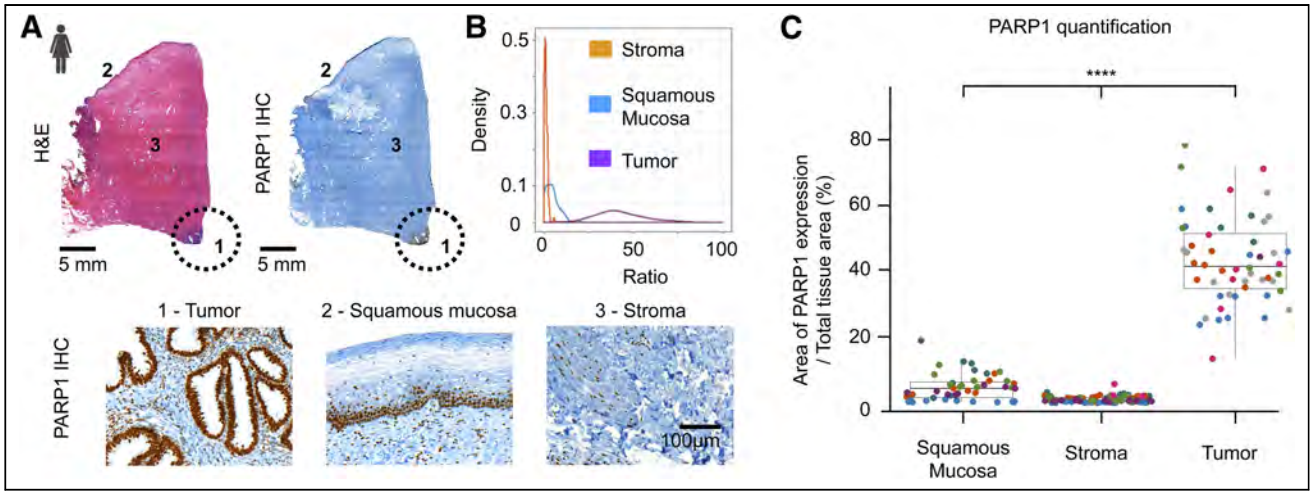

FIGURE 2. PARP1 expression on human cervical cancer banked tissue. (A) Tumor (cervical adenocarcinomas) and normal areas on H&E and immunohistochemistry patient slides. Circle demarcates tumor. Immunohistochemistry shows that PARP1 is highly expressed in adenocarcinoma but is much lower in normal stroma of benign squamous epithelium. (B) Density of ratio according to tissue type (*x*-axis truncated at 100 for visibility purposes). (C) Distribution of ratio according to tissue type (10 higher extreme values in tumor group were excluded for visibility purposes). Each color in graph represents a different patient ($n = 7$). Data in C are presented as mean ± SD. $^{*}P < 0.05$. $^{**}P < 0.01$. $^{***}P < 0.001$; $^{****}P < 0.0001$. IHC = immunohistochemistry.

observed a low PARPi-FL signal (31.57 ± 14.82 a.u.) and only a small number of sparse and small nuclei, which were visually distinct from tumor tissue. Each specimen underwent PARP1 immunohistochemistry, and the areas with increased PARP1 expression corresponded to the tumor seen on H&E. PARP1 expression was insignificant in the normal tissue, matching the observed levels of PARPi-FL. The tumor-to-background ratio of fluorescence in the histologically proven lesion versus normal tissue in the same specimen section from this patient was 2.65 (Fig. 4A). Patient 2 harbored an HPV-associated adenocarcinoma adjacent to a benign nabothian cyst (Fig. 4B), which can lead to overestimation of tumor volume on regular imaging. Confocal imaging of the tumor demonstrated cells with differently sized and shaped nuclei arranged in a highly disorganized manner. We did not observe any PARPi-FL uptake in the cyst wall or normal cervical mucosa. PARP1 expression corroborated the confocal imaging findings: higher expression was seen in the tumor, whereas almost no expression was present in the cyst or normal cervical mucosa. PARPi-FL emitted a signal of 105.8 ± 15.45 a.u. in the tumor. The signal was significantly higher than that in the normal adjacent mucosa (22.53 ± 2.95 a.u., $P < 0.0001$; Fig. 4B), yielding a tumor-to-background ratio of 4.69.

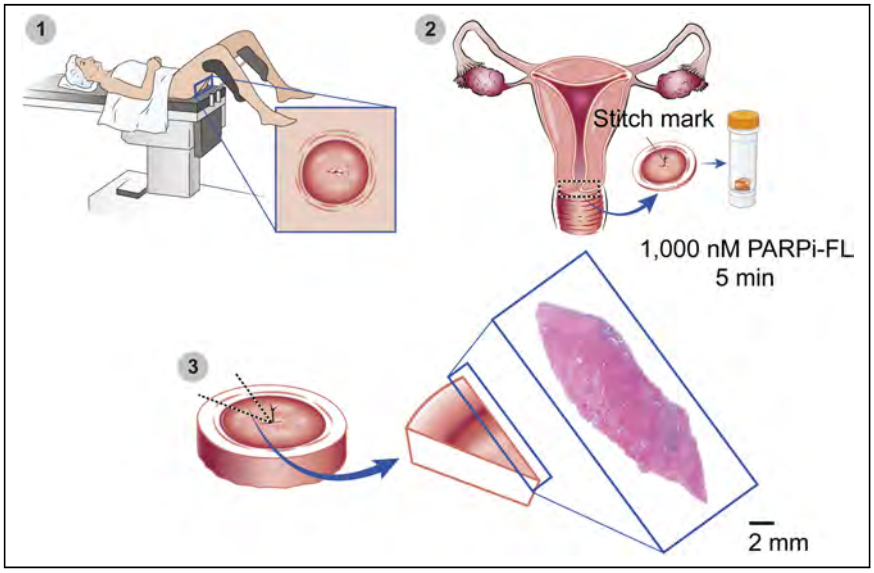

FIGURE 3. Experimental plan for patient's cone-biopsy biospecimen collection. (1) Cone biopsy samples from patients were resected and evaluated in operating room before standard-of-care processing. (2) Staining was performed on whole, freshly excised specimen by submersing tissue in solution containing 1,000 nM PARPi-FL solution in 15 mL of 30% PEG 300 in phosphate-buffered saline for 5 min (rapid staining protocol). Specimen was further washed in phosphate-buffered saline for 1 min before imaging. (3) After imaging, specimen was processed according to standard of care. Gynecologic pathologist confirmed histologic results and provided slides for study. Magnified image demonstrates how pathology slides were acquired.

We also imaged a patient with a low-grade squamous intraepithelial lesion (CIN type 1), an abnormal proliferation of immature squamous cells involving no more than the lower third of the squamous mucosa (Fig. 5). Handheld confocal microscopy of PARPi-FL showed organized tissue, with cells arranged in layers but with nuclei of different sizes and shapes (Fig. 5A). H&E staining showed a similar finding in the CIN type 1, with nuclei of varying sizes and shapes. PARP1 expression, and thus PARPi-FL uptake, were higher in the areas corresponding to disorganized tissue than in the healthy deeper stroma tissue. As usual in patients harboring CIN, this patient proved to be HPV-positive (Fig. 5B).

To demonstrate that the technique can also be used to image tumor cells in different gynecologic subsites, 1 patient with a

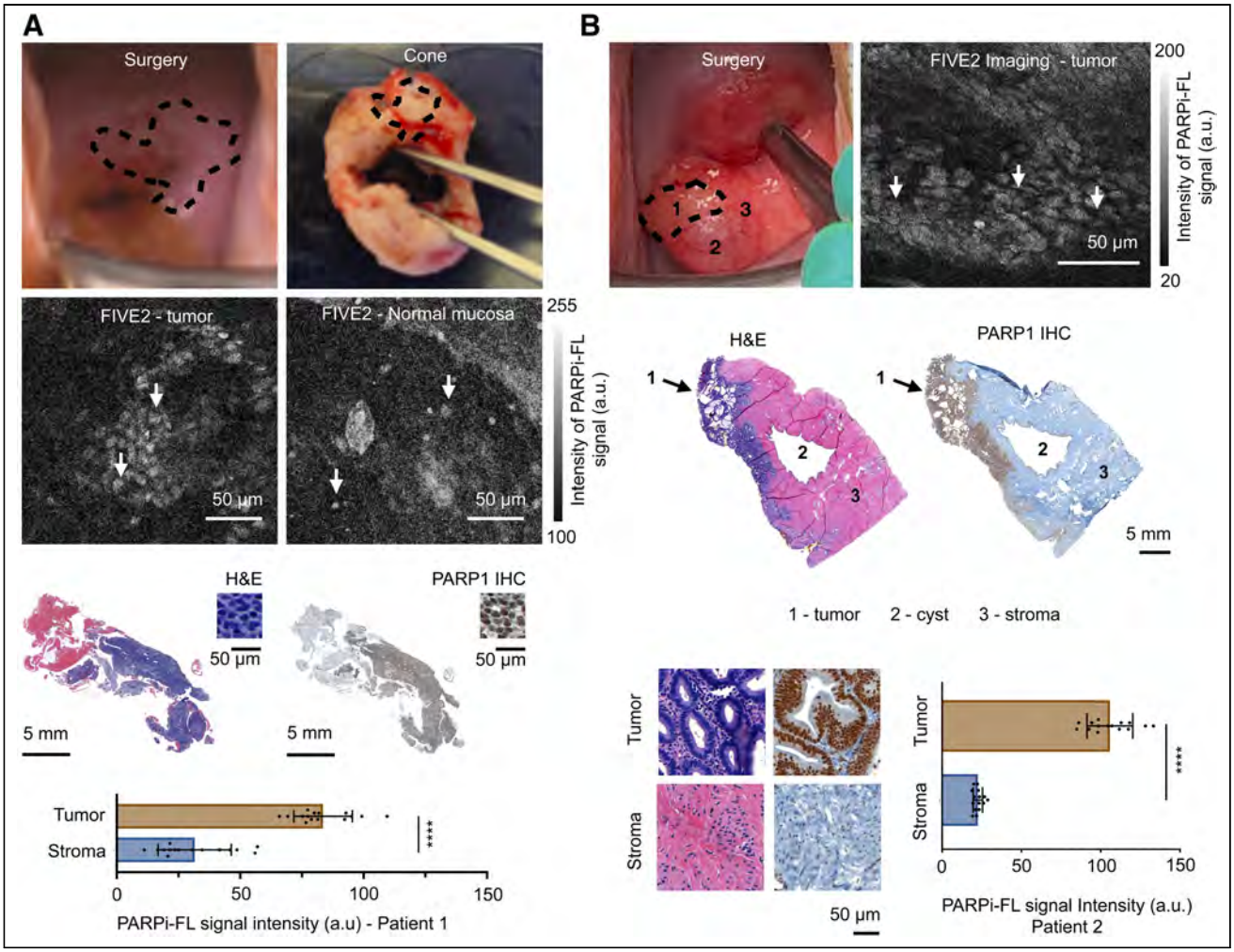

FIGURE 4. Imaging of cervical cancer with PARPi-FL stain and handheld confocal imaging in operating room before final pathology report for standard of care. (A) Patient 1 harbored adenocarcinoma of cervical transformation zone, extending to ectocervical mucosa. Dotted lines demarcate tumor. Second row shows tumor and healthy mucosa imaged by handheld confocal microscope at tissue depths of 13 and 8 μm, respectively. Images show cells arranged in disorganized manner and nuclei with different sizes and shapes. Arrows point to cell nuclei (average signal, 83.57 ± 11.85 a.u.), which were sparse and regularly shaped. Normal mucosa shows almost no PARPi-FL uptake (average signal, 22.53 ± 2.94 a.u.). H&E and PARP1 immunohistochemistry slides show areas of tumor with increased PARP1 expression. Almost no PARP1 expression is present in normal-tissue area. (B) Patient 2 harbored cervical adenocarcinoma, demarcated by dotted lines, adjacent to benign nabothian cyst. Numbers represent tumor (1), cyst (2), and normal stroma (3). Tissue depth is 3 μm. PARPi-FL emitted significantly higher signal in tumor than in normal surrounding mucosa (105.8 ± 14.45 and 22.53 ± 2.94 a.u., respectively; $P < 0.0001$). H&E and PARP1 immunohistochemistry staining confirmed presence of tumor. ****$P < 0.0001$. IHC = immunohistochemistry.

recurrent squamous cell carcinoma of the vulva invading the clitoris was imaged. The clitoris biospecimen was imaged using the same rapid staining protocol and imaging protocol, and the results were similar to the ones seen in the cervical cone biopsies: tumor presented with enlarged, variably-sized nuclei arranged in a disorganized manner, whereas the benign clitoral squamous mucosa (comprising most of the resected tissue) showed no PARPi-FL uptake (Fig. 6A). Histology and PARP1 immunohistochemistry corroborated the confocal findings, demonstrating that areas with no PARPi-FL signal corresponded to normal tissue whereas areas with nuclear signal corresponded to tumor (Fig. 6B). The quantification of PARPi-FL fluorescence signal was significantly ($P < 0.0001$) higher in the tumor area (98.07 ± 18.78 a.u.) than in the normal surrounding tissue (19.49 ± 11.97), yielding a tumor-to-background fluorescence ratio of 5.03.

DISCUSSION

PARP1 is an interesting target for tumor detection and delineation because of its increased expression in a large number of cancer types (*23*). Cancer is usually marked by genomic instability that is often the result of alterations in the signaling of the DNA repair chain (*24*). Several clinical trials are investigating the use of PARP inhibitors in different types of tumors, with promising results (*12*,*25*–*27*). Although no cutoff has been previously reported for determining when a lesion should be considered neoplastic by means of PARP1 expression, several papers have demonstrated that its increased expression can be used to differentiate tumors from their benign surrounding tissues (*17*,*23*,*28*,*29*). Similar to what has been previously published for other malignancies (*15*,*17*,*30*–*32*), PARP1 is overexpressed in cervical adenocarcinomas. The difference in PARP expression between tumor and benign tissue was so marked that tumor

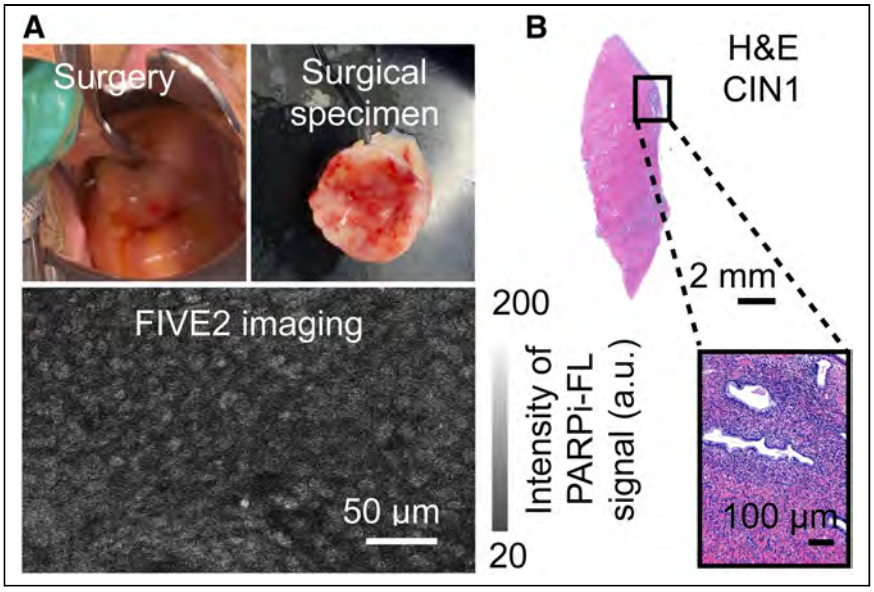

FIGURE 5. Imaging of cervical dysplasia with PARPI-FL stain and handheld confocal imaging in operating room before final pathology report. Standard-of-care assessment was used. (A) Patient harbored CIN type 1 of cervical os. Images from lesion demonstrated cells arranged in slightly disorganized manner, with nuclei of different sizes and shapes. Image depth is 4 µm. (B) Overview of specimen.

could be delineated solely on the basis of PARP quantification. Some tissues have physiologic PARP1 expression, especially those with high cellular turnover, such as the cervical squamous epithelium at the transformation zone. Thus, we have demonstrated that even though PARP1 expression is higher in cervical squamous mucosa than in stroma, it is significantly lower than in tumor. In this study, because of the low number of individuals, we did not consider the HPV status of patients for the purpose of imaging.

The ratio of PARP1 expression between tumor and normal tissue allowed visualization of cervical cancer cells, after staining with PARPi-FL, using a handheld confocal microscope. We demonstrated, using ex vivo fresh cone biopsy samples, that topical application of PARPi-FL on the cervix is feasible, is capable of identifying tumor cells, and can potentially lead to a novel diagnostic tool for fast tumor cell identification, allowing imaging of cervical cancer in real time.

In vivo confocal microscopy has been of great interest since it allows for visualization of abnormal tissue without the need for an incisional biopsy. Both fluorescence and reflectance confocal microscopy technologies are being studied in several other malignancies. We describe the use of a handheld fluorescence microscope equipped with a blue laser (excitation, 488; emission, >510) to detect the fluorescence signal arising from a contrast agent, PARPi-FL, that is specifically bound to PARP1 overexpressed in cancer cells. It is important to emphasize that PARPi-FL signal is in the green spectrum and that autofluorescence emission is also a component of the same spectrum. The broader autofluorescence peak width, however, allows us to separate specific (PARPi-FL) and nonspecific (autofluorescence) emissions. To achieve specific imaging, autofluorescence was being filtered using a band-pass filter (515–575 nm). PARPi-FL is able to maintain target affinity once it has been modified on the cyclopropane end of the olaparib scaffold, a region that is not essential for binding (*33–35*). Dyes in the near-infrared spectrum were

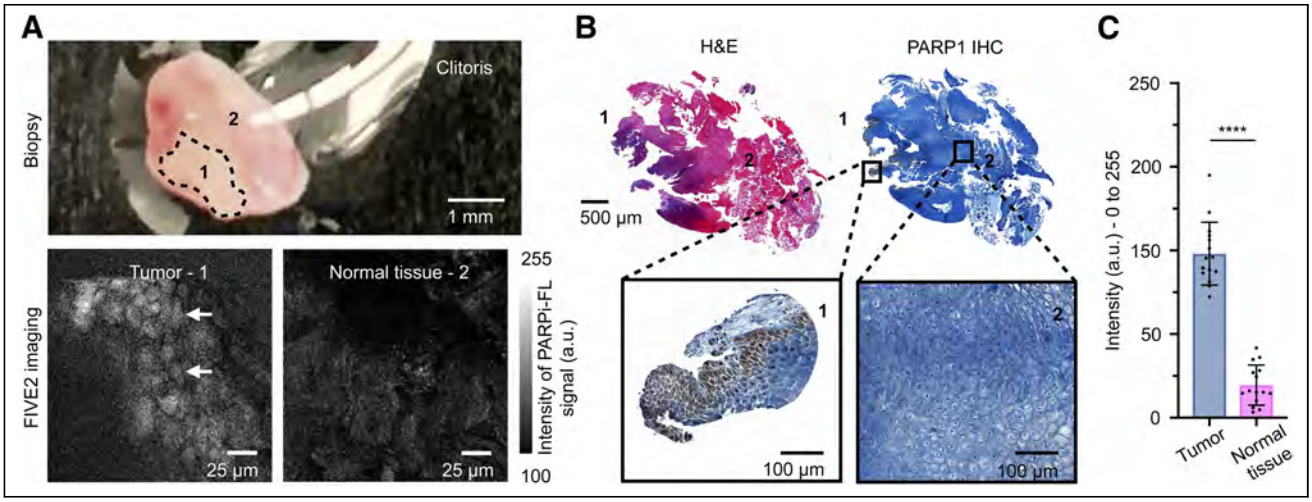

FIGURE 6. PARPi-FL imaging of excised clitoris with invasion from vulvar squamous cell carcinoma. (A) Patient biospecimen ex vivo. Dotted area (1) corresponds to tumor, and surrounding area (2) corresponds to benign margins. In bottom row, images acquired with handheld confocal microscope demonstrate tumor cells with enlarged nuclei that were different in size and arranged in very disorganized manner. Tissue depths are 4 µm in tumor and 6 µm in normal tissue. (B) H&E staining showed that tumor was restricted to small area in tissue, represented by number 1. PARP1 immunohistochemistry corroborated confocal findings since PARP1 expression was absent in stroma (2) but present in tumor (1). (C) Quantification of PARPi-FL uptake in tumor and normal tissue. Fluorescence signal was significantly ($P < 0.0001$) higher in tumor area than in normal surrounding tissue. ****$P < 0.0001$. IHC = immunohistochemistry.

previously investigated and reported but did not achieve similar binding (*36*,*37*).

Taking advantage of the PARP1 expression in the basal layer of cervical squamous epithelium, we confirmed, using a swine animal model, that PARPi-FL penetrates the tissue when applied topically. With minimal effort and time, its signal was detected by the handheld confocal microscope, allowing its use to obtain cellular resolution of the porcine cervix. As expected, the nuclei of normal tissue were considerably organized, with a homogeneous size and shape. When cone biopsy samples with tumor were imaged, PARPi-FL showed higher uptake in lesions than in surrounding normal tissue (Figs. 4 and 5), corresponding to PARP1 immunohistochemistry expression in those areas. The tumor cells showed a disorganized pattern and heterogeneously shaped nuclei, which were easily discernible through PARPi-FL staining.

In addition, the fact that we found PARPi-FL uptake in CIN type 1 is not surprising since PARP1 expression is present not only in the basal layer but also in squamous dysplasia (*15*). Importantly, different grades of cervical dysplasia are defined by the amount of immature squamous cell proliferation involving the mucosal thickness (CIN type 1, involving one third of the thickness of the epithelial layer; CIN type 2, involving one to two thirds; and CIN type 3, involving more than two thirds). Confocal microscopy picks up the fluorescent signal that arises from a single layer of cells (the *xy*-plane), which is ideal for cellularly resolving that layer and confirming the specificity of the probe. However, unless depth is considered as well (the *z*-plane), differentiating the grades of cervical dysplasia might be impractical. An associated technology, such as a handheld epifluorescence tool, that could integrate fluorescence arising from the total thickness of the dysplastic area would be a promising asset for distinguishing between the different grades of CIN and tumor. Additionally, PARPi-FL could be used to assess suspected lesions in real time or potentially replace acetic acid, serving as a more precise guide for biopsies or replacing the need for biopsy.

Lastly, although further studies are necessary to define the sensitivity and specificity of the tracer, our data suggest that PARPi-FL would work well for cancer screening during colposcopy procedures. It might also play a role in intraoperative imaging as a guide for tumor resection margins during loop electrosurgical excision or cone procedures, as the current approaches to determining the tumor boundaries rely on the expertise of the surgeon and, ultimately, the final pathology report. To date, no technology allows in vivo histologic determination of cervical lesions, and no intraoperative tumor marker is available to ensure clear margins, resulting in additional procedures should positive margins be noted in final pathology reports.

CONCLUSION

Contemporaneous and specific cellular visualization of cervical and clitoral cancer tissue was achieved using a topically applied fluorescent contrast agent, PARPi-FL, and a handheld fluorescence confocal microscope. This tracer has the potential to improve tumor identification on colposcopy examination by allowing real-time histology assessment.

DISCLOSURE

Susanne Kossatz, Snehal Patel, and Thomas Reiner are shareholders of Summit Biomedical Imaging and coinventors on filed U.S. patent WO2016164771, which covers methods for the use of PARPi-FL. Thomas Reiner is a coinventor on U.S. patent WO2012074840, covering the composition of matter for PARPi-FL, and is a paid consultant for Theragnostics, Inc. This work was supported by National Institutes of Health grants P30 CA008748, R01 CA204441 (Thomas Reiner), and R43 CA228815 (Thomas Reiner); the Molecularly Targeted Intra-Operative Imaging Fund of Memorial Sloan Kettering Cancer Center; the Department of Surgery at Memorial Sloan Kettering Funds; and the Memorial Sloan Kettering Imaging and Radiation Sciences Program. No other potential conflict of interest relevant to this article was reported.

ACKNOWLEDGMENTS

We gratefully acknowledge the support of Memorial Sloan Kettering's Animal Imaging Core, Radiochemistry and Molecular Imaging Probes Core, Molecular Cytology Core, Center for Molecular Imaging and Nanotechnology, and Animal Necropsy Core. We also thank Garon Scott for editing the manuscript and Drs. Christian Brand and Gary Peterson for helpful discussions.

KEY POINTS

QUESTION: Can the difference in PARP1 expression between tumor and normal tissue, and therefore PARPi-FL uptake, be observed when imaging cervical lesions?

PERTINENT FINDINGS: PARPi-FL is a topical fluorescent tracer that targets the PARP1 enzyme in the DNA repair chain, overexpressed in cervical adenocarcinoma. After topical application, PARPi-FL signal could be picked up by a handheld confocal microscope, allowing cellular resolution of cervical lesions.

IMPLICATIONS FOR PATIENT CARE: PARPi-FL signal can be picked up by a handheld confocal microscope, allowing cellular resolution of those lesions. We believe that our tracer has translational potential and might offer advantages over the current standard of care.

REFERENCES

1. Ferlay J, Colombet MSoerjomataram I, et al. Estimating the global cancer incidence and mortality in 2018: GLOBOCAN sources and methods. *Int J Cancer.* 2019;144:1941–1953.
2. Brisson M, Kim JJ, Canfell K, et al. Impact of HPV vaccination and cervical screening on cervical cancer elimination: a comparative modelling analysis in 78 low-income and lower-middle-income countries. Lancet. 2020;395:575–590.
3. Devarapalli P, Labani S, Nagarjuna N, Panchal P, Asthana S. Barriers affecting uptake of cervical cancer screening in low and middle income countries: a systematic review. *Indian J Cancer.* 2018;55:318–326.
4. Toliman PJ, Kaldor JM, Tabrizi SN, Vallely AJ. Innovative approaches to cervical cancer screening in low- and middle-income countries. *Climacteric.* 2018;21:235–238.
5. Parra SG, Rodriguez AM, Cherry KD, et al. Low-cost, high-resolution imaging for detecting cervical precancer in medically-underserved areas of Texas. *Gynecol Oncol.* 2019;154:558–564.
6. Parra S, Carranza E, Coole J, et al. Development of low-cost point-of-care technologies for cervical cancer prevention based on a single-board computer. *IEEE J Transl Eng Health Med.* 2020;8:4300210.
7. Pierce MC, Guan Y, Quinn MK, et al. A pilot study of low-cost, high-resolution microendoscopy as a tool for identifying women with cervical precancer. *Cancer Prev Res (Phila).* 2012;5:1273–1279.
8. Mariano VS, Lorenzi AT, Scapulatempo-Neto C, et al. A low-cost HPV immunochromatographic assay to detect high-grade cervical intraepithelial neoplasia. *PLoS One.* 2016;11:e0164892.
9. Rodriguez NM, Wong WS, Liu L, Dewar R, Klapperich CM. A fully integrated paperfluidic molecular diagnostic chip for the extraction, amplification, and detection of nucleic acids from clinical samples. *Lab Chip.* 2016;16:753–763.

10. Catarino R, Schafer S, Vassilakos P, Petignat P, Arbyn M. Accuracy of combinations of visual inspection using acetic acid or Lugol iodine to detect cervical precancer: a meta-analysis. *BJOG.* 2018;125:545–553.
11. Parham GP, Mwanahamuntu MH, Kapambwe S, et al. Population-level scale-up of cervical cancer prevention services in a low-resource setting: development, implementation, and evaluation of the cervical cancer prevention program in Zambia. *PLoS One.* 2015;10:e0122169.
12. Boussios S, Karihtala P, Moschetta M, et al. Combined strategies with poly (ADP-ribose) polymerase (PARP) inhibitors for the treatment of ovarian cancer: a literature review. *Diagnostics (Basel).* 2019;9:87.
13. Pujade-Lauraine E, Ledermann JA, Selle F, et al. Olaparib tablets as maintenance therapy in patients with platinum-sensitive, relapsed ovarian cancer and a BRCA1/2 mutation (SOLO2/ENGOT-Ov21): a double-blind, randomised, placebo-controlled, phase 3 trial. *Lancet Oncol.* 2017;18:1274–1284.
14. Kossatz S, Weber WA, Reiner T. Optical imaging of PARP1 in response to radiation in oral squamous cell carcinoma. *PLoS One.* 2016;11:e0147752.
15. Kossatz S, Pirovano G, Demetrio De Souza Franca P, et al. Validation of the use of a fluorescent PARP1 inhibitor for the detection of oral, oropharyngeal and oesophageal epithelial cancers. *Nat Biomed Eng.* 2020;4:272–285.
16. Chow JP, Man WY, Mao M, et al. PARP1 is overexpressed in nasopharyngeal carcinoma and its inhibition enhances radiotherapy. *Mol Cancer Ther.* 2013;12:2517–2528.
17. Demétrio de Souza Franca P, Roberts S, Kossatz S, et al. Fluorine-18 labeled poly (ADP-ribose) polymerase1 inhibitor as a potential alternative to 2-deoxy-2-[^{18}F]fluoro-D-glucose positron emission tomography in oral cancer imaging. *Nucl Med Biol.* 2020;84-85:80–87.
18. Kossatz S, Brand C, Gutiontov S, et al. Detection and delineation of oral cancer with a PARP1 targeted optical imaging agent. *Sci Rep.* 2016;6:21371.
19. Thurber GM, Yang KS, Reiner T, et al. Single-cell and subcellular pharmacokinetic imaging allows insight into drug action in vivo. *Nat Commun.* 2013;4:1504.
20. Carney B, Kossatz S, Reiner T. Molecular imaging of PARP. *J Nucl Med.* 2017;58:1025–1030.
21. Zhu W, Pirovano G, O'Neal PK, et al. Smartphone epifluorescence microscopy for cellular imaging of fresh tissue in low-resource settings. *Biomed Opt Express.* 2019;11:89–98.
22. Reiner T, Lacy J, Keliher EJ, et al. Imaging therapeutic PARP inhibition in vivo through bioorthogonally developed companion imaging agents. *Neoplasia.* 2012;14:169–177.
23. Tang J, Salloum D, Carney B, et al. Targeted PET imaging strategy to differentiate malignant from inflamed lymph nodes in diffuse large B-cell lymphoma. *Proc Natl Acad Sci USA.* 2017;114:E7441–E7449.
24. Mateo J, Lord CJ, Serra V, et al. A decade of clinical development of PARP inhibitors in perspective. *Ann Oncol.* 2019;30:1437–1447.
25. Wilson RH, Evans TJ, Middleton MR, et al. A phase I study of intravenous and oral rucaparib in combination with chemotherapy in patients with advanced solid tumours. *Br J Cancer.* 2017;116:884–892.
26. Litton JK, Rugo HS, Ettl J, et al. Talazoparib in patients with advanced breast cancer and a germline BRCA mutation. *N Engl J Med.* 2018;379:753–763.
27. Clarke N, Wiechno P, Alekseev B, et al. Olaparib combined with abiraterone in patients with metastatic castration-resistant prostate cancer: a randomised, double-blind, placebo-controlled, phase 2 trial. *Lancet Oncol.* 2018;19:975–986.
28. Schöder HM, Demetrio De Souza Franca P, Nakajima R, et al. Safety and feasibility of PARP1/2 imaging with 18F-PARPi in patients with head and neck cancer. *Clin Cancer Res.* 2020;26:3110–3116.
29. Pirovano G, Jannetti SA, Carter LM, et al. Targeted brain tumor radiotherapy using an auger emitter. *Clin Cancer Res.* 2020;26:2871–2781.
30. Carney B, Kossatz S, Lok BH, et al. Target engagement imaging of PARP inhibitors in small-cell lung cancer. *Nat Commun.* 2018;9:176.
31. Zhou D, Xu J, Mpoy C, et al. Preliminary evaluation of a novel ^{18}F-labeled PARP-1 ligand for PET imaging of PARP-1 expression in prostate cancer. *Nucl Med Biol.* 2018;66:26–31.
32. Pirovano G, Jannetti SA, Carter LM, et al. Targeted brain tumor radiotherapy using an Auger emitter. *Clin Cancer Res.* 2020;26:2871–2881.
33. Carney B, Kossatz S, Reiner T. Molecular imaging of PARP. *J Nucl Med.* 2017;58:1025–1030.
34. Dubach JM, Kim E, Yang K, et al. Quantitating drug-target engagement in single cells in vitro and in vivo. *Nat Chem Biol.* 2017;13:168–173.
35. Dubach JM, Vinegoni C, Mazitschek R, Fumene Feruglio P, Cameron LA, Weissleder R. In vivo imaging of specific drug-target binding at subcellular resolution. *Nat Commun.* 2014;5:3946.
36. Thurber GM, Reiner T, Yang KS, Kohler RH, Weissleder R. Effect of small-molecule modification on single-cell pharmacokinetics of PARP inhibitors. *Mol Cancer Ther.* 2014;13:986–995.
37. Demétrio de Souza França P, Guru N, Roberts S, et al. Fluorescence-guided resection of tumors in mouse models of oral cancer. *Sci Rep.* 2020;10:11175.